Long-range superconducting proximity effect in YBa2Cu3O7/La0.7Ca0.3MnO3 weak-link arrays

D. Sanchez-Manzano, S. Mesoraca, S. Rodriguez-Corvillo, A. Lagarrigue, F. Gallego, F. Cuellar, A. Sander, A. Rivera-Calzada, S. Valencia, Javier Villegas, et al.

Long-range superconducting proximity effect in $YBa_2Cu_3O_7/La_{0.7}Ca_{0.3}MnO_3$ weak-link arrays

D. Sanchez-Manzano[1*], S. Mesoraca[2], S. Rodriguez-Corvillo[1], A. Lagarrigue[2], F. Gallego[1], F. A. Cuellar[1], A. Sander[2], A. Rivera-Calzada[1], S. Valencia[3], J.E. Villegas[2], C. Leon[1], J. Santamaria[1]

[1] GFMC, Departamento de Física de Materiales, Facultad de Ciencias Físicas, UCM, Plaza Ciencias, 1 28040, Madrid, Spain

[2] Unité Mixte de Physique, CNRS, Thales, Université Paris-Saclay, 91767, Palaiseau, France

[3] Helmholtz-Zentrum Berlin für Materialien und Energie, Albert-Einstein-Str. 15, 12489 Berlin, Germany

* Corresponding author. davidsan@ucm.es

Abstract

The interplay between ferromagnetism and superconductivity has attracted substantial interest due to its potential for exotic quantum phenomena and advanced electronic devices. Although ferromagnetism and superconductivity are antagonistic phenomena, ferromagnets (F) can host spin-triplet superconductivity induced via proximity with superconductors (S). Up to now, most of the experimental effort has been focused on single S/F/S junctions. Here we have found the fingerprints of long-range superconducting proximity effect in micrometric weak-link arrays, formed by embedding $YBa_2Cu_3O_7$ superconducting islands in a half-metallic ferromagnet $La_{0.7}Ca_{0.3}MnO_3$ film. These arrays show magnetoresistance oscillations that appear at temperatures below the critical temperature of $YBa_2Cu_3O_7$ for currents below a threshold, indicating their superconducting origin. This realization paves the way to device architectures displaying macroscopic quantum interference effects, of interest for field sensing applications among others.

The possible coexistence of ferromagnetism and superconductivity has attracted interest for many years[1]. Singlet superconductivity (SC) and ferromagnetism (FM) are antagonistic phenomena because the exchange field of a F tends to spin-polarize Cooper pairs' electrons with opposite spins. The recent discovery of superconductivity in a P-doped $EuFe_2As_2$ compound[2] with extremely weak exchange interaction between electrons and localized moments is a rare case of coexistence of ferromagnetism and singlet superconductivity. Another possibility for F/S coexistence is spin-triplet superconductivity. Here, equal-spin Cooper pairs can survive over long distances in ferromagnets. Triplet pairing is also very rare as an intrinsic phenomenon, and has only been observed in uranium compounds[3–6]. However, it has been theoretically and experimentally demonstrated that triplet correlations can emerge at the interface between a ferromagnet (F) and a superconductor (S) resulting from the presence of inhomogeneous magnetization[7–9], non-collinear magnetizations in ferromagnetic multilayers[10,11], and spin-dependent scattering or momentum-dependent exchange fields due to the spin-orbit interaction[12–14]. In experiments with both conventional low-temperature superconductors and high-temperature superconductors, supercurrents have been observed across S-F-S junctions in which F thickness is in the tens of nanometer range[15–20], significantly exceeding the expectations for the singlet S-F proximity effect, thereby supporting the triplet scenario. Additionally, lateral (planar) devices based on half-metallic ferromagnets (like CrO_2 and $La_{0.7}Sr_{0.3}MnO_3$) have exhibited supercurrents decaying over even longer distances, up to micrometers, which strongly indicates proximity-induced triplet superconductivity[21–25]. All those realizations have paved the way to the so-called superconducting spintronics. This research field, at the intersection of superconductivity and ferromagnetism, has garnered significant attention due to its potential for quantum computing[26] and sensing[17], and for the exploration of exotic quantum phenomena[27].

Most of the studies on S/F proximity effects have focused on individual S/F/S junctions and multilayers, Yet, for nonmagnetic systems, a different type of 2-dimensional (2D) proximity structures has been explored which consists of superconducting islands embedded e.g. on metallic[28], semiconducting[29,30] or insulating films[31]. In these structures, superconductivity is induced around the superconducting islands by proximity effect, which allows the global propagation of superconducting correlations across all the

embedding material, the space between the S islands behaving as weak links. Such 2D weak-link arrays constitute an interesting platform for studying a variety of physics problems that span from Berezinskii-Kosterlitz-Thouless (BKT) transitions to dimensional or geometric frustration effects[32,33]. In this paper, we explore the long-range superconducting proximity effect in 2D weak-link in which the proximitized materials is a ferromagnet. In particular, we investigate arrays based on the high-temperature superconductor $YBa_2Cu_3O_7$ (YBCO) and the half-metallic ferromagnetic $La_{0.7}Ca_{0.3}MnO_3$ (LCMO). We find macroscopic superconducting quantum interference effects that dominate magnetotransport despite the very long (micrometer) separation between superconducting islands, thus highlighting the presence of triplet superconductivity. We believe this class of 2D weak-link arrays, based of triplet superconductivity, offers much potential for manipulation of superconductivity based on the spin degree of freedom, which bears both significant fundamental and technological interests.

In this study, we have used a simple approach to fabricate $YBa_2Cu_3O_7/La_{0.7}Ca_{0.3}MnO_3$ planar weak link arrays. To do so, a single layer of YBCO (24 nm) was grown on top of $SrTiO_3$ (001) by high-oxygen pressure sputtering at 900ºC at $P(O_2) = 3.4$ mbar followed by a 30-minute baking at 550ºC at $P(O_2) =$ 900 mbar. Subsequently, a 19x19 matrix of YBCO micropillars was defined using conventional photolithography and wet etching. The micropillars are 3.5 x 3.5 μm^2 in size and are separated L=1.33 μm. Figure 1c displays AFM image of the YBCO micropillars, which appear well separated excluding the presence of shorts between them. On top of this matrix, a single layer of LCMO (d=30nm) was deposited using the same sputtering growth process used for YBCO. Figure 1a shows a side-view schematic of the resulting device indicating the dimensions. Figure 1b shows a top view of the device, featuring the 4-points measurement configuration employed to measure magnetoresistance. In this configuration, current flows across several YBCO micropillars and their respective LCMO spacers, and magnetic field is applied perpendicular to current direction.

The resistance vs temperature of the device is depicted in Figure 1d. The sharp drop of the resistance at 87.5 K signals the T_c of YBCO. Above it, we observe two maxima of the resistance related to the presence of LCMO. For a LCMO single layer only one maximum is expected for its characteristic insulator-to-metal transition of LCMO[34]. The presence of two maxima suggests the existence of two

LCMO phases with different metal-to-insulator transitions (MIT), one at T_{MIT}= 230 K, close to the one expected for the optimally doped thin layers[34] and a second one, extremely suppressed, at T_{MIT}=130 K, which might be attributed to variations in the growth process of LCMO (on either STO or YBCO surfaces) or potential oxygen migration between LCMO and the ab-planes of YBCO.

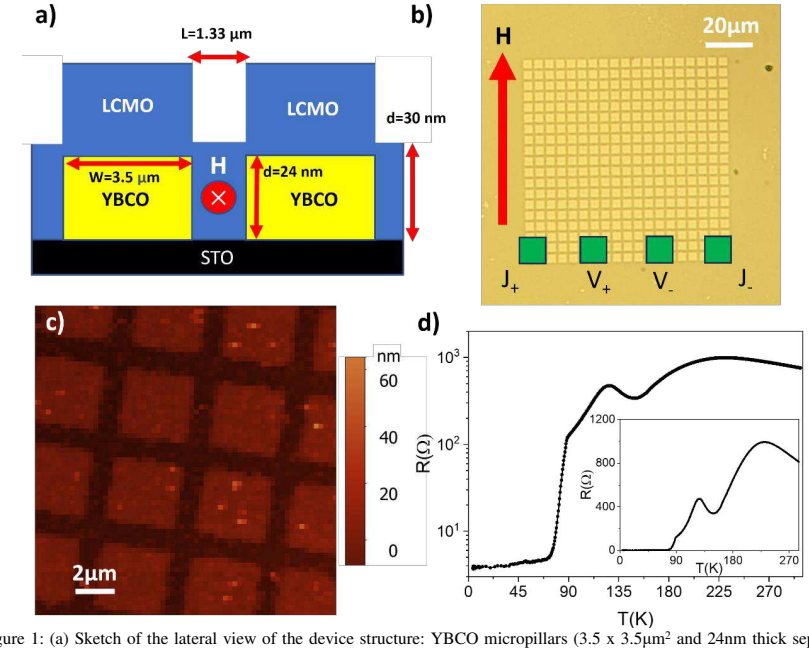

Figure 1: (a) Sketch of the lateral view of the device structure: YBCO micropillars (3.5 x 3.5µm^2 and 24nm thick separated 1.33µm) matrix, in yellow, covered by a single layer of LCMO (30nm), in blue. Central red circle indicates the direction of the field. Current is injected left to right. (b) Measurement configuration and optical microscope image of the device. Green squares indicate where the sputtered gold contacts were deposited to inject current and measure voltage. (c) AFM image of a representative part of the matrix, showing the separation between YBCO micropillars. (d) Resistance versus temperature of the device with a current level of 10 µA. Both the MIT of LCMO and the superconducting transition of YBCO can be observed. Inset: RvsT in linear scale, highlighting the two MITs of LCMO.

To further investigate whether these two FM phases are intermixed or spatially separated, we imaged the magnetic domain structure of the S/F array as function of temperature. We employed photoemission electron microscopy (PEEM), using X-ray magnetic circular dichroism (XMCD) as magnetic contrast mechanism. The angle of incidence of the incoming X-ray beam is set to 16° with respect to the sample surface with its in-plane projection parallel to the (010) LCMO direction (parallel to one of the edges of the YBCO squares). This configuration ensures large sensitivity to the in-plane magnetization. Images of the array were obtained at the Mn L_3 edge (640.3eV) with incoming left (σ^-) and right (σ^+) circularly polarized radiation. The XMCD is computed as XMCD = $(\sigma^- - \sigma^+) / (\sigma^- + \sigma^+)$. The blue (red) color scale

used to illustrate the resulting XMCD images highlights magnetization parallel (anti-parallel) to the X-ray beam propagation direction. White colored regions, corresponding to XMCD = 0, result from regions with zero magnetization or with the magnetization orthogonal to the beam propagation direction. XMCD images were obtained at remanence for different temperatures after applying a 1000 Oe magnetic field pulse (1s) at T=55K, along the (010) direction. The results are shown in Figure 2. The temperature dependent XMCD reveals the existence of two spatially separated ferromagnetic LCMO phases in our system: the LCMO layer on top of YBCO displays a higher Curie temperature, T_{Curie} (between 240 K and 160 K) compared to the LCMO located between YBCO micropillars (with T_{Curie} between 145K and 100K). The XMCD analysis validates the observation from resistance measurements of the presence of two different T_{MIT}, as T_{MIT} and T_{Curie} are linked in manganites[35,36]. It is essential to emphasize that all the LCMO remains ferromagnetic well above and below the critical temperature (87K) of YBCO.

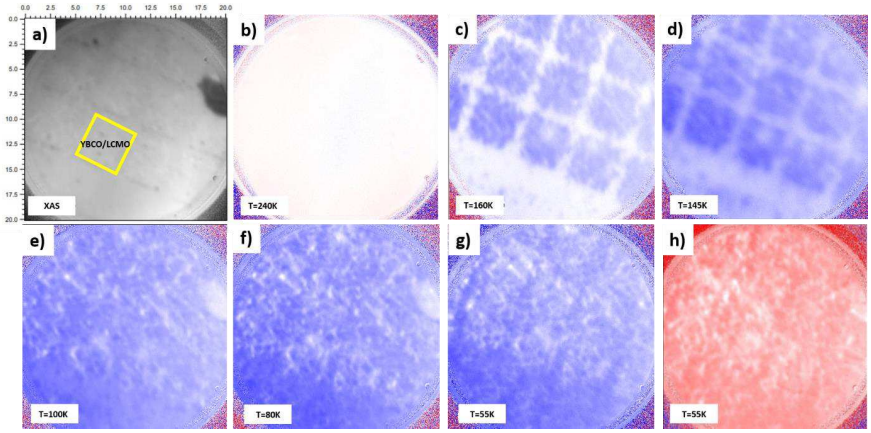

Figure 2: (a) XAS of the zone to be measured. (b) to (g) XMCD signal evolution in function of temperature after application of 1000 Oe in plane, measured in remanence. Two Curie temperatures can be clearly observed, the one of the LCMO on top of the YBCO and the one of LCMO between YBCO and outside of the YBCO matrix. (h) Reversal of the magnetization after applying -1000Oe in plane, measured in remanence.

For a better understanding of the magnetic characteristics of the system, magnetoresistance curves were measured above and below the critical temperature of YBCO. Figure 3a displays the magnetoresistance at 90K, which shows the expected behavior for a LCMO films[37], anisotropic low-field magnetoresistance (AMR) features (with peaks indicating a coercive field of 20 mT) combined with the negative magnetoresistance background at high field, which corresponds to the colossal magnetoresistance (CMR). Remarkably, as the temperature is decreased cooled below 15 K, the

magnetoresistance reveals an oscillating pattern, superimposed on the LCMO magnetoresistance, with a periodicity of 37 mT (Figure 3b). For this composition of the manganite the low temperature phase is homogeneous, i.e., it does not show phase separation which is known to be pronounced for other manganites[38]. Here, the only source of inhomogeneity is at the metal to insulator transition, away from the temperature range of the observed resistance oscillations.

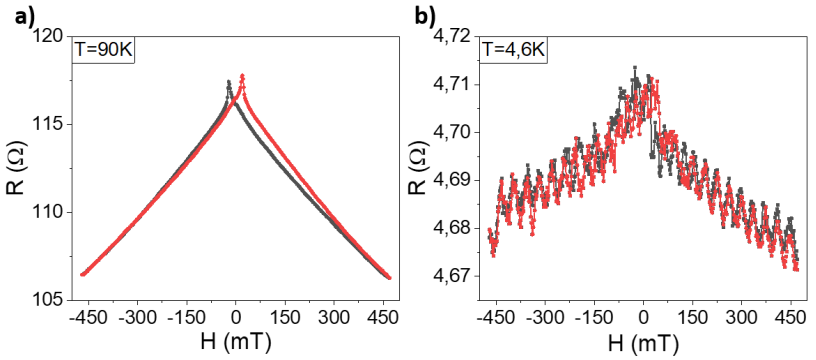

Figure 3: (a) Magnetoresistance curves with magnetic field applied in plane above Tc of YBCO with I=60μA. A typical LCMO magnetoresistance curve is observed, with coercive fields close to 20mT. (b) Magnetoresistance curves with magnetic field applied in plane for below the Tc of YBCO. Fraunhofer like oscillations appear, showing a small hysteretic behavior only at low fields.

Furthermore, the amplitude of the oscillations decreases by increasing either the applied current (above 260 μA) or the temperature (above T=19 K) of the system, while maintaining the same periodicity (Figure 4a and 4b). This behavior suggests a superconducting origin of these oscillations.

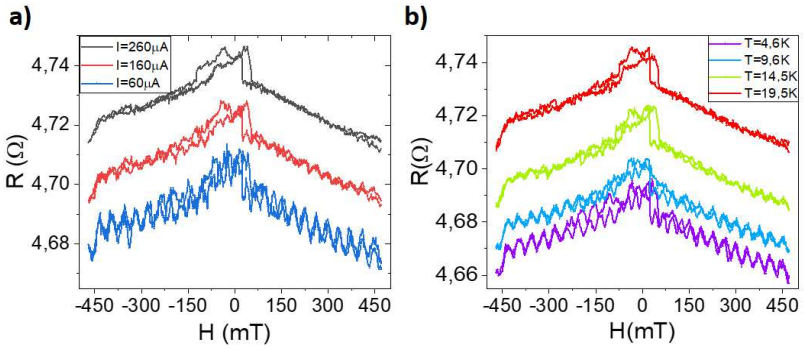

Figure 4: Magnetoresistance oscillations with a 37mT period appear below a certain (a) current (at T= 5K) and (b) temperature threshold (with I=50μA). In both cases, the amplitude of the oscillations fades away when either current (a) or temperature (b) is increased.

The abrupt resistance drop observed when temperature is reduced below the critical temperature of YBCO (see Figure 1d) is a strong indication of the ferromagnetic/superconducting proximity effect on the LCMO layers. As we discuss in what follows, this resistance drop can only be understood if we assume a strong suppression of the LCMO resistance below that temperature. To probe it, we estimate the expected resistance values at 100 K and 4 K in the case of no proximity effect. We start from typical resistivity values for YBCO and LCMO. We will assume that the resistivity of LCMO[34] at 100 K is $\rho_{T=100K}$= 0.35 mΩ·cm and at 4 K $\rho_{T=4K}$= 0.2 mΩ·cm, and that the resistivity of YBCO is $\rho_{T=100K}$= 0.07 mΩ·cm in the normal-state and $\rho_{T=4K}$= 0 mΩ·cm in the superconducting state, according to measurements done in single layers. Considering that voltage is measured across three YBCO/LCMO micropillars (with LCMO and YBCO components connected in parallel) connected in series through the LCMO spacer (see measurement configuration shown in Figure 1a and 1b and Supplementary Material Figure S1), we have estimated the resistance at different temperatures with the following formula: $R_{Total} = N \cdot \left(R_{LCMO\,1}{}_{/_{YBCO}} + R_{LCMO\,2}\right) = N \cdot \left(\frac{R_{LCMO\,1}+R_{YBCO}}{R R_{LCMO\,1} \cdot R_{YBCO}} + R_{LCMO\,2}\right)$ where $R_{LCMO\,1}$ is the resistance of the LCMO on top of YBCO, R_{YBCO} the resistance of YBCO and $R_{LCMO\,2}$ the resistance of the LCMO spacer. N is the total number of devices (i.e. one YBCO/LCMO micropillar connected in series with 1 LCMO spacer). Each resistance is calculated taking into account the resistivity at different temperatures and the dimensions of the devices (as shown in Figure 1a).

At 100K, the unit cell formed by the bilayer-spacer is expected to have a R= 67 Ω. Since our measurement configuration involves N=3 micropillars (see Figure 1b), the total resistance at 100 K would be $R_{T=100K}$ =201 Ω, a value close to the one experimentally measured $R_{m,T=100K}$ =186 Ω. At 4 K, with the YBCO resistance now reduced to zero, the resistance of the unit cell would be solely due to the LCMO layer. The estimated value is $R_{T=4K}$ = 76 Ω, more than one order of magnitude higher than the measured $R_{m,T=4K}$ ~ 4 Ω. Even considering a possible conduction in parallel across the 3x3 set of micropillars covered by the contacts, the low temperature resistance state ($R_{T=4K}$=25 Ω) would still be one order of magnitude above the measured value. This significant difference between the estimated and measured resistances can only be understood if the resistance of the LCMO spacer in between the YBCO/LCMO pillars is significantly reduced by superconducting proximity effect. In contrast to

previous experiments[23–25], our study did not reveal a zero resistance state, which suggests inhomogeneities across the array[28]. Because the array has multiple YBCO/LCMO/YBCO junctions connected in series, a weaker superconducting proximity effect in one of the junctions along the current path could mask the effects of fully proximized junctions. Another possible explanation for the absence of zero resistance, may be related to degradation of the YBCO micropillars at the edges upon etching (see Figure 1c). This degradation may result in a decrease of the T_c at the interface in contact with the LCMO, thereby weakening the efficiency of the proximity effect.

One important indication of superconducting proximity effect is found in the oscillations observed in the magnetoresistance curves. The critical current of a Josephson junction oscillates with magnetic field according to the well-known Fraunhofer pattern: $I_c(H) = I_{c0}\left|\frac{\sin \pi\frac{\Phi}{\Phi_0}}{\pi\frac{\Phi}{\Phi_0}}\right|$, where $\Phi(H) = \mu_0 H A_{eff}$ is the fmagnetic flux threaded by the junction, I_{c0} is the maximum critical current and Φ_0 the flux quantum (2.07×10^{-15} Wb). In fact, the (magnetic field) period of 37 mT of the oscillations observed, corresponds to a weak link area of 0.056 μm^2, which fairly matches the geometry of the LCMO spacers between YBCO pillars. The effective area of the weak link, i.e., the LCMO in between YBCO micropillars (Figure 1a) can be calculated $A_{eff} = (L + 2\lambda) \cdot d = 0.055\ \mu m^2$, by assuming a value of λ=250 nm for the London penetration depth of YBCO when in contact with LCMO[23]. The good agreement between the expected and the measured effective area demonstrates the superconducting nature of the oscillations. As observed, increasing either temperature of current level decreases the amplitude of the oscillations, making them eventually disappear as expected from the reduction of the critical current. It is important to notice that these oscillations are not dampened while increasing field. This type of behaviour is expected in Josephson junctions with an inhomogeneous current distribution[39]. For our measurement configuration, the critical current should flow through the upper and lower edges of the LCMO weak link (see Figure 1a). In fact, a similar effect has been observed in Nb/Co/Nb[40] triplet Josephson junctions, where the long-range triplet correlations appear only in highly localized channels at the edge of the ferromagnet. Fermin et al.[40] proposed that this effect is due to the presence of an effective spin-orbit coupling (SOC), originated via non-collinear spin textures present at the barrier[41,42].

This spin-orbit coupling can lead to the appearance of equilibrium triplet Cooper pair spin currents flowing through the edges of the barrier[40,43]. This behavior provides further confirmation of the triplet weak link Josephson junction characteristics in our system, even across a relatively long barrier (1.33 μm) of ferromagnetic LCMO and with smaller widths (3.5μm) of SC/FM interfaces to generate triplet supercurrents, contrary to our previous works in which their large width could make it difficult to understand how triplet supercurrents are generated.

In summary, we have shown evidence of magnetic flux quantization effects in the resistance of $YBa_2Cu_3O_7/La_{0.7}Ca_{0.3}MnO_3$ weak-link arrays which can be extinguished by either increasing applied current or temperature. We rationalize these results in terms of a triplet superconducting proximity effect over the micron wide LCMO spacers (1.33 μm) between YBCO micro squares of the array. The matrix of proximized LCMO weak links signals a promising avenue for advanced quantum sensing or logic devices[44] incorporating the spin degree of freedom[45,46]. Overall, the combination of ferromagnets and superconductors in weak link arrays holds great promise for practical applications in information processing and beyond.

Supplementary Material

See the supplementary material for a sketch of the resistors' configuration used to calculate the resistance at T=100K and T=4K.

Work at UCM supported by Agencia Estatal de Investigación through PID2020-118078RB-I00, TED 2021-130196B-C21, and by Comunidad de Madrid Y2020-NMT6661 (CAIRO). We thank Helmholtz-Zentrum Berlin for the allocation of synchrotron radiation beamtime supported by the project CALIPSOplus under the Grant Agreement 730872 from the EU Framework Programme for Research and Innovation HORIZON 2020. Work at CNRS/Thales supported by French ANR "SUPERFAST", EU-FLAG-ERA "To2Dox" and COST action "SUPERQUMAP".

References

[1] P.W. Anderson, and H. Suhl, "Spin Alignment in the Superconducting State," Physical Review **116**(4), 898 (1959).

[2] V.S. Stolyarov, I.S. Veshchunov, S.Y. Grebenchuk, D.S. Baranov, I.A. Golovchanskiy, A.G. Shishkin, N. Zhou, Z. Shi, X. Xu, S. Pyon, Y. Sun, W. Jiao, G.H. Cao, L.Y. Vinnikov, A.A. Golubov, T. Tamegai, A.I. Buzdin, and D. Roditchev, "Domain Meissner state and spontaneous vortex-antivortex generation in the ferromagnetic superconductor EuFe2(As0.79P0.21)2," Sci Adv **4**(7), (2018).

[3] D. Aoki, and Jaques Flouquet, "Ferromagnetism and Superconductivity in Uranium Compounds," J Appl Phys **81**(011003), 1–11 (2012).

[4] D. Aoki, A. Huxley, E. Ressouche, D. Braithwaite, J. Flouquet, J.-P. Brison, E. Lhotel, and C. Paulsen, "Coexistence of superconductivity and ferromagnetism in URhGe," Nature **413**(6856), 613–616 (2001).

[5] L. Jiao, S. Howard, S. Ran, Z. Wang, J.O. Rodriguez, M. Sigrist, Z. Wang, N.P. Butch, and V. Madhavan, "Chiral superconductivity in heavy-fermion metal UTe2," Nature **579**(7800), 523–527 (2020).

[6] S. Ran, C. Eckberg, Q.P. Ding, Y. Furukawa, T. Metz, S.R. Saha, I.L. Liu, M. Zic, H. Kim, J. Paglione, and N.P. Butch, "Nearly ferromagnetic spin-triplet superconductivity," Science (1979) **365**(6454), 684–687 (2019).

[7] M. Eschrig, and T. Löfwander, "Triplet supercurrents in clean and disordered half-metallic ferromagnets," Nat Phys **4**(2), 138–143 (2008).

[8] M. Eschrig, "Spin-polarized supercurrents for spintronics: A review of current progress," Reports on Progress in Physics **78**(10), 104501 (2015).

[9] M. Eschrig, J. Kopu, J.C. Cuevas, and G. Schön, "Theory of Half-Metal/Superconductor Heterostructures," Phys Rev Lett **90**(13), 4 (2003).

[10] M. Houzet, and A.I. Buzdin, "Long range triplet Josephson effect through a ferromagnetic trilayer," Phys Rev B Condens Matter Mater Phys **76**(6), 060504 (2007).

[11] C. Richard, M. Houzet, and J.S. Meyer, "Superharmonic long-range triplet current in a diffusive Josephson junction," Phys Rev Lett **110**(21), 1–5 (2013).

[12] F.S. Bergeret, A.F. Volkov, and K.B. Efetov, "Long-range proximity effects in superconductor-ferromagnet structures," Phys Rev Lett **86**(18), 4096–4099 (2001).

[13] F.S. Bergeret, A.F. Volkov, and K.B. Efetov, "Odd triplet superconductivity and related phenomena in superconductor- ferromagnet structures," Rev Mod Phys **77**(4), 1321–1373 (2005).

[14] F.S. Bergeret, and I. V. Tokatly, "Singlet-triplet conversion and the long-range proximity effect in superconductor-ferromagnet structures with generic spin dependent fields," Phys Rev Lett **110**(11), 1–6 (2013).

[15] J.W. A Robinson, J.D. S Witt, and M.G. Blamire, "Controlled Injection of Spin-Triplet Supercurrents into a Strong Ferromagnet," Science (1979) **329**(5987), 59–61 (2010).

[16] T.S. Khaire, M.A. Khasawneh, W.P. Pratt, and N.O. Birge, "Observation of spin-triplet superconductivity in co-based josephson junctions," Phys Rev Lett **104**(13), (2010).

[17] E.C. Gingrich, B.M. Niedzielski, J.A. Glick, Y. Wang, D.L. Miller, R. Loloee, W.P. Pratt, and N.O. Birge, "Controllable 0-π Josephson junctions containing a ferromagnetic spin valve," Nat Phys **12**(6), 564–567 (2016).

[18] C. Visani, Z. Sefrioui, J. Tornos, C. Leon, J. Briatico, M. Bibes, a. Barthélémy, J. Santamaría, and J.E. Villegas, "Equal-spin Andreev reflection and long-range coherent transport in high-temperature superconductor/half-metallic ferromagnet junctions," Nat Phys **8**(7), 539–543 (2012).

[19] Y. Kalcheim, T. Kirzhner, G. Koren, and O. Millo, "Long-range proximity effect in La2/3Ca1/3MnO 3/(100)YBa2Cu3O7-δ ferromagnet/superconductor bilayers: Evidence for induced triplet superconductivity in the ferromagnet," Phys Rev B Condens Matter Mater Phys **83**(6), 2–7 (2011).

[20] K. Dybko, K. Werner-Malento, P. Aleshkevych, M. Wojcik, M. Sawicki, and P. Przyslupski, "Possible spin.triplet superconducting phase in the La0.7Sr0.3MnO3/YBa2Cu3O7/La0.7Sr0.3MnO3 trilayer," Phys Rev B Condens Matter Mater Phys **80**(14), 0–9 (2009).

[21] R.S. Keizer, S.T.B. Goennenwein, T.M. Klapwijk, G. Miao, G. Xiao, and A. Gupta, "A spin triplet supercurrent through the half-metallic ferromagnet CrO 2," Nature **439**(7078), 825–827 (2006).

[22] M.S. Anwar, F. Czeschka, M. Hesselberth, M. Porcu, and J. Aarts, "Long-range supercurrents through half-metallic ferromagnetic CrO 2," Phys Rev B Condens Matter Mater Phys **82**(10), 2–5 (2010).

[23] D. Sanchez-Manzano, S. Mesoraca, F.A. Cuellar, M. Cabero, V. Rouco, G. Orfila, X. Palermo, A. Balan, L. Marcano, A. Sander, M. Rocci, J. Garcia-Barriocanal, F. Gallego, J. Tornos, A. Rivera, F. Mompean, M. Garcia-Hernandez, J.M. Gonzalez-Calbet, C. Leon, S. Valencia, C. Feuillet-Palma, N. Bergeal, A.I. Buzdin, J. Lesueur, J.E. Villegas, and J. Santamaria, "Extremely long-range, high-temperature Josephson coupling across a half-metallic ferromagnet," Nature Materials 2021 21:2 **21**(2), 188–194 (2022).

[24] D. Sanchez-Manzano, S. Mesoraca, F. Cuellar, M. Cabero, S. Rodriguez-Corvillo, V. Rouco, F. Mompean, M. Garcia-Hernandez, J.M. Gonzalez-Calbet, C. Feuillet-Palma, N. Bergeal, J. Lesueur, C. Leon, J.E. Villegas, and J. Santamaria, "Unconventional long range triplet proximity effect in planar YBa2Cu3O7/La0.7Sr0.3MnO3/YBa2Cu3O7 Josephson junctions," Supercond Sci Technol **36**(7), 074002 (2023).

[25] Y. Jungxiang, R. Fermin, K. Lahabi, and J. Aarts, "Triplet supercurrents in lateral Josephson junctions with a half-metallic ferromagnet," ArXiv:2303.13922v1, (2023).

[26] T. Yamashita, K. Tanikawa, S. Takahashi, and S. Maekawa, "Superconducting π qubit with a ferromagnetic Josephson junction," Phys Rev Lett **95**(9), 1–4 (2005).

[27] J. Linder, and J.W.A. Robinson, "Superconducting spintronics," Nat Phys **11**(4), 307–315 (2015).

[28] S. Eley, S. Gopalakrishnan, P.M. Goldbart, and N. Mason, "Approaching zero-temperature metallic states in mesoscopic superconductor–normal–superconductor arrays," Nature Physics 8:1 **8**(1), 59–62 (2012).

[29] Z. Han, A. Allain, H. Arjmandi-Tash, K. Tikhonov, M. Feigel'Man, B. Sacépé, and V. Bouchiat, "Collapse of superconductivity in a hybrid tin–graphene Josephson junction array," Nature Physics 10:5 **10**(5), 380–386 (2014).

[30] C.G.L. Bøttcher, F. Nichele, M. Kjaergaard, H.J. Suominen, J. Shabani, C.J. Palmstrøm, and C.M. Marcus, "Superconducting, insulating and anomalous metallic regimes in a gated two-dimensional semiconductor–superconductor array," Nat Phys **14**(11), 1138–1144 (2018).

[31] S. Mukhopadhyay, J. Senior, J. Saez-Mollejo, D. Puglia, M. Zemlicka, J.M. Fink, and A.P. Higginbotham, "Superconductivity from a melted insulator in Josephson junction arrays," Nature Physics 2023, 1–6 (2023).

[32] D.J. Resnick, J.C. Garland, J.T. Boyd, S. Shoemaker, and R.S. Newrock, "Kosterlitz-thouless transition in proximity-coupled superconducting arrays," Phys Rev Lett **47**(21), 1542–1545 (1981).

[33] D.W. Abraham, C.J. Lobb, M. Tinkham, and T.M. Klapwijk, "Resistive transition in two-dimensional arrays of superconducting weak links," Phys Rev B **26**(9), 5268–5271 (1982).

[34] N.M. Nemes, M. García-Hernández, Z. Szatmári, T. Fehér, F. Simon, C. Visani, V. Peña, C. Miller, J. García-Barriocanal, F. Bruno, Z. Sefrioui, C. Leon, and J. Santamaría, "Thickness dependent magnetic anisotropy of ultrathin LCMO epitaxial thin films," IEEE Trans Magn **44**(11 PART 2), 2926–2929 (2008).

[35] A. Urushibara, Y. Moritomo, T. Arima, A. Asamitsu, G. Kido, and Y. Tokura, "Insulator-metal transition and giant magnetoresistance in La1-xSrxMnO3," Phys Rev B **51**(20), 14103 (1995).

[36] M.B. Salamon, and M. Jaime, "The physics of manganites: Structure and transport," Rev Mod Phys **73**(3), 583 (2001).

[37] M. Ziese, ; H C Semmelhack, ; K H Han, ; S P Sena, ; H J Blythe,) H C Semmelhack, K.H. Han, S.P. Sena, and H.J. Blythe, "Thickness dependent magnetic and magnetotransport properties of strain-relaxed La0.7Ca0.3MnO3 films," J Appl Phys **91**(12), 9930–9936 (2002).

[38] K.A. Moler, "Imaging quantum materials," Nat Mater **16**(11), 1049–1052 (2017).

[39] A. Barone, and G. Paternò, "Physics and Applications of the Josephson Effect," Physics and Applications of the Josephson Effect, (1982).

[40] R. Fermin, D. Van Dinter, M. Hubert, B. Woltjes, M. Silaev, J. Aarts, and K. Lahabi, "Superconducting Triplet Rim Currents in a Spin-Textured Ferromagnetic Disk," Nano Lett **22**(6), 2209–2216 (2022).

[41] I. V. Bobkova, and Y.S. Barash, "Effects of spin-orbit interaction on superconductor-ferromagnet heterostructures: Spontaneous electric and spin surface currents," JETP Lett **80**(7), 494–499 (2004).

[42] F.S. Bergeret, and I. V. Tokatly, "Singlet-triplet conversion and the long-range proximity effect in superconductor-ferromagnet structures with generic spin dependent fields," Phys Rev Lett **110**(11), 117003 (2013).

[43] F.S. Bergeret, and I. V. Tokatly, "Spin-orbit coupling as a source of long-range triplet proximity effect in superconductor-ferromagnet hybrid structures," Phys Rev B Condens Matter Mater Phys **89**(13), 134517 (2014).

[44] L.B. Ioffe, M. V. Feigel'man, A. Ioselevich, D. Ivanov, M. Troyer, and G. Blatter, "Topologically protected quantum bits using Josephson junction arrays," Nature 2002 415:6871 **415**(6871), 503–506 (2002).

[45] J. Oppenländer, C. Häussler, and N. Schopohl, "Non − Φ 0 − periodic macroscopic quantum interference in one-dimensional parallel Josephson junction arrays with unconventional grating structure," Phys Rev B **63**(2), 024511 (2000).

[46] F. Couëdo, E. Recoba Pawlowski, J. Kermorvant, J. Trastoy, D. Crété, Y. Lemaître, B. Marcilhac, C. Ulysse, C. Feuillet-Palma, N. Bergeal, and J. Lesueur, "High-TC superconducting detector for highly-sensitive microwave magnetometry," Appl Phys Lett **114**(19), 192602 (2019).